Internal Energy Distributions Resulting from Sustained Off-Resonance Excitation in Fourier Transform Ion Cyclotron Resonance Mass Spectrometry. II. Fragmentation of the 1-Bromonaphthalene Radical Cation

Julia Laskin* and Jean Futrell

Pacific Northwest National Laboratory, William R. Wiley Environmental Molecular Sciences Laboratory, P.O. Box 999 (K8-96), Richland, Washington 99352

Received: January 24, 2000; In Final Form: March 23, 2000

The collision energy dependence of the fragmentation of the 1-bromonaphthalene radical cation was studied using sustained off-resonance excitation (SORI) in a 7 T Fourier transform ion cyclotron resonance mass spectrometer (FTMS). Fragmentation efficiency curves were obtained as a function of collision energy at four different pressures of Ar bath gas corresponding to collision numbers of 3, 5, 15, and 20. The results were modeled using RRKM/QET formalism. A refined analytical form for the collisional energy deposition function is proposed. The ability to obtain accurate fragmentation energetics of a complex system using the present approach is demonstrated. The "effective temperatures" deduced from the average internal energies for $C_6H_5Br^{+\bullet}$ and $C_{10}H_7Br^{+\bullet}$ were found to be the same for both ions provided the bath gas pressure and the maximum value of center-of-mass collision energy were the same. The range of effective temperatures from 1000 to 3700 K sampled in the present study significantly exceeds the temperature range accessible by blackbody infrared radiative dissociation (BIRD). We anticipate that the present approach can be used to study fragmentation energetics of biomolecules.

Introduction

Collision-induced dissociation (CID) is a powerful tool both for determination of ion structures in the gas phase and for obtaining information on energetics and mechanisms of fragmentation processes of internally excited ions. Principles of collisional activation (CA) as well as various aspects and challenges of CA of polyatomic ions have been extensively discussed in several recent reviews.[1−4]

The present study is a continuation of our group's ongoing research focused on characterizing the energy deposition function following sustained off-resonance irradiation CID (SORI-CID) in Fourier transform ion cyclotron resonance mass spectrometer (FTMS). Collisional activation in FTMS can be implemented using either on-resonance or off-resonance excitation of the precursor ion. In the former case, ions are accelerated to a desired kinetic energy with a short radio frequency (rf) pulse applied at the cyclotron frequency of the precursor ion[5,6] and activated by collisions with neutral atoms or molecules inside the ICR cell. This technique has been used to study fragmentation of relatively small ions under single-collision conditions. If multiple collisions occur, the kinetic energy of ions is effectively damped, and the efficiency of subsequent collisions is small. However, multiple collisions are clearly required to induce substantial fragmentation of large molecules (e.g., protonated peptides and proteins). Fragmentation efficiency of large molecules is limited by both (1) the decrease in the center-of-mass (CM) collision energy with increase in the mass of the precursor ion and (2) the dramatic decrease in decomposition rates with increase in the number of internal degrees of freedom.

Several variations of conventional on-resonance excitation have been developed to enhance fragmentation of large molecules and improve the collection efficiency of product ions generated by multiple-collision activation. In multiple excitation collisional activation (MECA),[7,8] precursor ions that do not dissociate after the first excitation step are re-excited several times until dissociation occurs. Fragmentation efficiency is significantly improved using this method. Furthermore, lower kinetic energies, which will leave product ions closer to the center of the cell, can be used in MECA compared with conventional CID. Sustained off-resonance irradiation (SORI)[9] makes use of an off-resonance excitation of the ion being investigated. An rf pulse is applied slightly above or below the resonant frequency of the precursor ion causing the kinetic energy of the ion to oscillate with time. Because ion kinetic energy oscillates with time and collisions occur randomly, the collision frequency at the maximum number density of the gas pulse should be high enough to sample the full center-of-mass energy range and effectively average over all kinetic energies. For quantitative analysis of collision energy-resolved mass spectra, the collision frequency should also be low enough to avoid effective damping of the ion kinetic energy by collisions.[47] To ensure multiple collisions, the excitation pulse is applied for a time much larger than the time between collisions. With multiple collisions of translationally excited ions with the target gas, its internal energy slowly increases and fragmentation occurs when sufficient energy is transferred from translational to internal energy. Similar ideas are utilized in very-low-energy collisional activation (VLE-CA).[10,11] In this method, sequential acceleration/deceleration is achieved using a 180° phase shift of the excitation waveform. Because of its high fragmentation efficiency and relatively simple implementation, SORI−CID

* Corresponding author. E-mail: Julia.Laskin@pnl.gov; FAX: (509)-376-3650.

10.1021/jp000281x CCC: $19.00
Published on Web 05/16/2000

is the most widely used method. Most of SORI−CID studies carried out so far were focused on sequencing of peptides or improving our understanding of dissociation mechanisms based on the fragmentation patterns of different precursor ions.

Quantitative information on the energetics and dynamics of the observed fragmentation pathways can be obtained if we know the internal energy distribution of collisionally activated precursor ions. Various activation methods, including collision-induced dissociation under single collision conditions,[12] surface-induced dissociation (SID),[13,14] infrared multiphoton dissociation (IRMPD)[15] combined with FTMS, and boundary-activated dissociation (BAD)[16] implemented in a quadrupole ion trap have been used to study the energetics of fragmentation of large molecules (e.g., peptides). However, the internal energy distribution of ions activated using these techniques is usually poorly defined. Blackbody infrared dissociation (BIRD)[17−20] has been the most successful method thus far for studying the energetics of fragmentation of large molecules. This method utilizes the photon flux generated by the vacuum chamber walls and the long time scale of FTMS to heat the ions radiatively and to follow their fragmentation as a function of wall temperature. It has been shown that large ions can equilibrate with the blackbody radiation field and have internal energies given by a Boltzmann distribution. Arrhenius parameters for the dissociation of a variety of small ions, peptides, and proteins have been reported.[18−23]

The advantage of SORI−CID over the BIRD technique is that a much wider range of "effective temperatures" can easily be reached using SORI−CID. Accordingly several groups have studied energy deposition following SORI excitation. Schnier et al. have determined "effective temperatures" of protonated leucine enkephalin and doubly protonated bradykinin by comparing the dissociation kinetics following SORI−CID with that obtained under BIRD conditions.[24] They found that the effective temperatures of both peptides dissociated under the same SORI−CID conditions are similar. This observation is very encouraging because it points to the potential to use SORI excitation for quantitative analysis of the fragmentation of large molecules. The influence of different experimental parameters on the effective temperature was investigated. Fujiwara and Naito simulated internal energy distribution following SORI−CID of singly protonated bradykinin with argon using the Monte Carlo method.[25] Maximum internal energy of ∼11 eV was obtained from the simulation for a peak-to-peak excitation voltage of 2 V, frequency offset of 250 Hz, and pulse duration of 20 ms. The maximum internal energy of the precursor ion was found to be inversely proportional to the $\Delta\nu^3$, where $\Delta\nu$ is the frequency offset of the excitation wave.

We recently carried out an extensive study of collision-induced dissociation of $C_6H_5Br^+$ using both on-resonance and SORI excitation.[26] Fragmentation efficiency curves were obtained as a function of collision energy under single- and multiple- collision conditions. The results were modeled using RRKM/QET formalism. An analytical form for the collisional energy deposition function (CEDF) was proposed. Experimental results obtained over a wide range of experimental parameters (e.g., collision energies and pressures) were modeled using the same analytical form of the CEDF. An exponential energy deposition function gave the best fit to the single-collision experiment, whereas multiple-collision experiments were reproduced by a Boltzmann-like CEDF. We demonstrated that large amounts of internal energy can be deposited into the ion with SORI excitation, such that the energetics of fragmentation of both low- and high-energy channels can be investigated. Further, the ability to extract thermochemical information from SORI−CID measurements was demonstrated by RRKM-based modeling in which the amount of fragmentation observed is related to internal energy content rather than to the initial kinetic energy of the molecular ion (which is poorly defined).

Here we present a detailed study of the fragmentation of the 1-bromonaphthalene radical cation following SORI excitation. Collision energy-resolved fragmentation efficiency curves were analyzed to determine (1) the energetics of different fragmentation pathways of the molecular ion, (2) the amount of energy deposited into the ion, and (3) the change in the internal energy distribution as a function of collision energy and number of collisions. We show the ability of the method to provide valuable information on the energetics and dynamics of fragmentation of a relatively complex system. Average energies and "effective temperatures" obtained from the model are compared with the results obtained for $C_6H_5Br^{+\bullet}$ in our previous study.[26]

Experimental Section

The experimental conditions for well-defined collision energy-resolved SORI−CID measurements were described by us recently.[26] Experiments were performed on the University of Delaware 7T Bruker BioApex FT-ICR mass spectrometer equipped with an infinity cell. The system is operated at an indicated base pressure of 5×10^{-10} Torr. Ions generated in an external electron-impact ionization source were transferred into the ICR cell by a series of ion transfer lenses and captured in the cell using the Sidekick mechanism for ion accumulation. Ions were trapped in the cell by applying a 2 V potential to the trapping plates. Excess kinetic energy was removed from the ions by pulsing Ar into the cell for a duration of ∼300 ms at a maximum pressure of 2×10^{-6} Torr. Ions were allowed to cool to thermal equilibrium by radiative and collisional cooling during the pumping delay of 5 to 10 s. The precursor ion was isolated using a correlated sweep procedure. A second Ar pulse was then introduced to remove any excess kinetic energy gained by the molecular ions during the isolation event.

A third Ar pulse was introduced into the cell for collisional activation. We have measured the time-dependent pressure of Ar in the cell previously.[26] The pressure profile shows a peak in pressure at ∼100−120 ms delay time between the pulse valve opening and detection event and full width at half-maximum (fwhm) of ∼170 ms. Ion activation was performed during the time when the pressure was close to its maximum. Ions of *m*/*z* 206 were radially excited slightly off-resonance ($\Delta f = -700$ Hz) for 100 ms at nearly fixed Ar pressure. Pressure calibration described by us previously[26] was used throughout this work. The kinetic energy of the ions was incremented by changing the peak-to-peak voltage applied to the excitation plates. After a 5-s pumping delay, the ions were excited for detection by broadband chirp excitation.

The maximum center-of-mass (CM) energy achieved using SORI excitation is given by: [26]

$$E_{CM}^{max} = \left(\frac{M}{M+m}\right)\frac{\beta^2 q^2 V_{p-p}^2}{32\pi^2 m d^2 \Delta f^2}$$

where m and q are the mass and the charge of the ion, respectively, M is the mass of the neutral molecule, β is the geometry factor of the ICR cell ($\beta = 0.9$ for the infinity cell employed in this study), V_{p-p} is the peak-to-peak excitation voltage, d is the diameter of the ICR cell, and Δf is the shift of the SORI excitation frequency relative to the cyclotron frequency of the precursor ion.

From the set of spectra obtained at different collision energies, a plot of the relative precursor and fragment ion abundance as a function of the maximum CM energy of the precursor ion was constructed. We refer to these curves as fragmentation efficiency curves (FECs). We have recently demonstrated that the distribution of the number of collisions for the SORI excitation is asymmetric, with much higher weight for small collision numbers.[26] Consequently, the average number of collisions is smaller than the collision number characteristic of that distribution. FECs were measured at four different pressures corresponding to collision numbers of 3, 5, 15, and 20 and average numbers of collisions encountered by a precursor ion during SORI excitation of 1.9, 3.2, 6.3, and 9.5, respectively. (Note that the ions undergo 70 oscillations during the excitation period, and the maximum collision frequency utilized in our experiments is much lower than the frequency of SORI oscillations).

Double-resonance experiments combined with SORI excitation were performed by applying an additional rf wave, simultaneously with the SORI excitation pulse, with a frequency corresponding to the cyclotron frequency of the ion to be ejected and an amplitude of 50 V. The duration of the ejecting pulse (typically 3 s) was chosen to be long enough to allow ejection of the ions formed both during the SORI excitation pulse and after the excitation wave has been switched off.

We also conducted a limited number of non-FTMS experiments. Linked B^2/E scans and mass-analyzed ion kinetic-energy spectroscopy (MIKEs) studies were carried out on a Micromass ZabSpec/orthogonal TOF instrument in this laboratory. All experiments utilized 1-bromonaphthalene with a stated purity of 98%, purchased from Aldrich.

Results and Discussion

Collision Energy-Resolved Mass Spectra. Collision energy-resolved SORI−CID spectra were obtained at four different pressures corresponding to collision numbers of 3, 5, 15, and 20, respectively. The evolution of the mass spectrum as a function of CM collision energy for collision numbers $a = 5$ and 15 is presented in Figures 1a and 1b, respectively. As expected, more extensive fragmentation is obtained at higher pressure. In the high-pressure regime, the parent ion intensity becomes <1% already at 6 eV, whereas in the low-pressure experiment, even at the highest CM energy (14 eV), >40% of the parent ion population remains intact. The major fragments obtained in both experiments are *m*/*z* 127, 126, 101, 77, 75, 74, 51, and 50. However, in the high-pressure case, more high-energy fragments are observed (*m*/*z* 99, 98, 87, 86, 73, 63, and 62). These ions are not observed in the low-pressure experiment.

Dissociation Pathways. Double-resonance experiments were performed to verify dissociation pathways of bromonaphthalene and its fragments. In these experiments, a selected fragment is continuously ejected from the ICR cell during the SORI excitation. The ejecting rf wave is continued for an additional 3 s after the SORI excitation pulse is turned off to ensure a complete ejection of all the ions of the selected mass-to-charge ratio. As a result of ejection of a particular fragment ion, intensities of all the ions for which it is a precursor are strongly reduced. These experiments were performed with the SORI excitation voltage that corresponds to a maximum center-of-mass collision energy of 15 eV and Ar pressure corresponding to a collision number of 20. Under these CID conditions all the fragment ions of interest are present in a normal SORI−CID spectrum.

Although double-resonance ejection is, in principle, a straightforward method for determining precursor ion/daughter ion relationships, in practice it requires a compromise for rf amplitude setting. The amplitude of the ejecting wave should be low enough to avoid translational off-resonance excitation of adjacent masses and high enough to ensure a complete ejection and minimize unimolecular or collision-induced decay of the precursor ion during ejection. Fragmentation during ejection becomes particularly pronounced for SORI−CID performed at high collision energies where fragmentation time could become shorter than the time required for ion ejection. For example, ejection time corresponding to the peak-to-peak voltage of 50 V utilized in the present study is ∼1 ms, and all fragments produced in this time interval appear in the mass spectrum despite continuous ejection of their precursor ion. Increasing the amplitude of the ejection wave (thereby reducing the ejection time) caused considerable off-resonance excitation of the peaks separated by one mass unit from the ion being ejected.

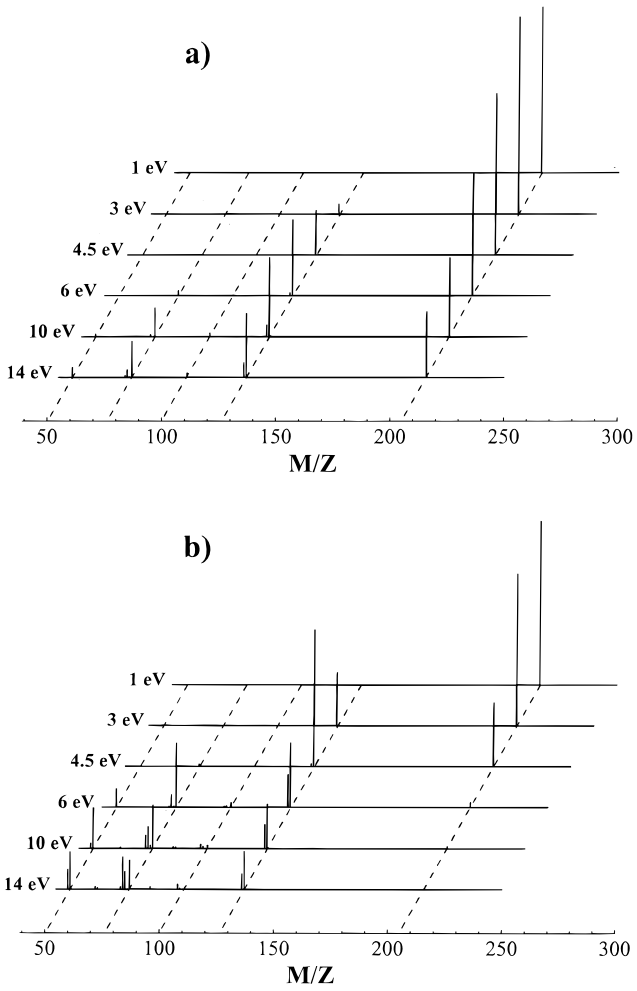

Figure 1. Evolution of SORI−CID spectrum as a function of maximum CM collision energy for two different pressures: (a) $a = 5$; (b) $a = 15$.

The ion intensities in double-resonance experiments were normalized to the intensity of the parent ion, $C_{10}H_7Br^{+\bullet}$, which is not affected by the ejection procedure. When naphthyl cation ($C_{10}H_7^+$) is continuously ejected from the cell, the intensities of all other fragment ions are reduced to a few percent of their original intensities. This result indicates that this fragment ion is produced directly from the molecular ion and the rest of the fragments are formed by subsequent fragmentation of $C_{10}H_7^+$. Ejection of $C_8H_5^+$ (*m*/*z* 101) affects the intensities of two smaller

fragments of *m*/*z* 75 and 74. The *m*/*z* 51 and 50 fragments are eliminated when *m*/*z* 77 is continuously ejected. All remaining fragments are suppressed when $C_{10}H_6^{+\bullet}$ is ejected. These observations are summarized in the mechanism shown below as Scheme 1.

SCHEME 1

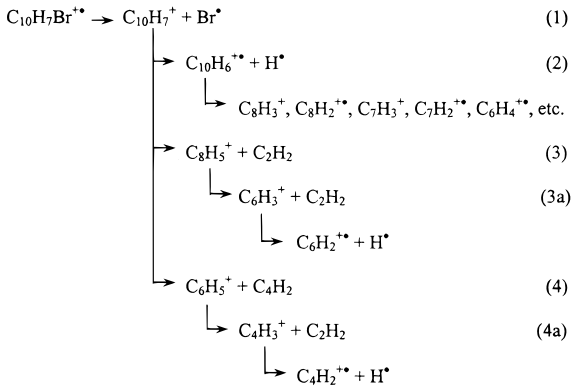

That Scheme 1 accurately represents the decomposition of naphthyl bromide radical cation is further substantiated by the MIKEs study described later.

As shown, naphthyl cation fragments via a loss of hydrogen (reaction 2), C_2H_2 (reaction 3), and C_4H_2 (reaction 4). Product ions formed by reactions 3 and 4 ($C_8H_5^+$ and $C_6H_5^+$) fragment by a subsequent loss of C_2H_2 with a further hydrogen elimination, whereas a variety of product ions are formed from $C_{10}H_6^{+\bullet}$. The reactions that are numbered in Scheme 1 (1−4a) will be considered in the RRKM modeling of the naphthyl bromide dissociation process.

Linked B^2/E scans and mass-analyzed ion kinetic-energy spectroscopy (MIKEs) studies were carried out on a sector mass spectrometer to verify the proposed fragmentation scheme. Examples of MIKEs spectra of $C_{10}H_6^{+\bullet}$ (*m*/*z* 126), $C_8H_5^+$ (*m*/*z* 101), and $C_6H_5^+$ (*m*/*z* 77) are presented in Figures 2 (a−c). These measurements confirm that $C_8H_5^+$ and $C_6H_5^+$ lose C_2H_2 to give $C_6H_3^+$ (*m*/*z* 75) and $C_4H_3^+$ (*m*/*z* 51), respectively. $C_6H_4^+$ (*m*/*z* 76) is a major fragment formed from $C_{10}H_6^{+\bullet}$, which is in agreement with the results of double-resonance experiments. However, another major fragment formed from $C_{10}H_6^{+\bullet}$, corresponding to the loss of acetylene (*m*/*z* 100), was not observed in our FTMS experiments. This apparent contradiction can be rationalized in terms of the well-known energy−entropy tradeoff. Because of the long reaction time sampled by FTMS, SORI−CID spectra are mainly determined by the energetics of fragmentation. However, both energetics (the critical energy for reaction) and dynamics (the activation entropy) are important in MIKEs spectra, which sample a much shorter reaction time (∼30 μs) and which sample higher internal energies of precursor ions. At these energies, dissociation processes proceeding via a loose transition state and having high critical energy for dissociation can compete efficiently with reactions that have lower critical energy but proceed via a tight transition state. Significant differences between MIKE and SORI−CID spectra can arise from the differences in the internal energy distributions of the fragmenting ions as well as from entropy effect. Consider, for example, the rate−energy curves for two competing reactions both proceeding via a loose transition state. These curves are essentially parallel, and the relative abundance of the fragments is insensitive to the shape of the internal energy distribution function and the observation time. If, on the other hand one reaction proceeds via a tight transition state and the other via a loose transition state, the branching ratio of the products is strongly dependent on the internal energy content of the precursor ion. For pronounced differences in entropy−acute intersection of rate-energy curves−competition is effectively observed only in a very narrow window of internal energies

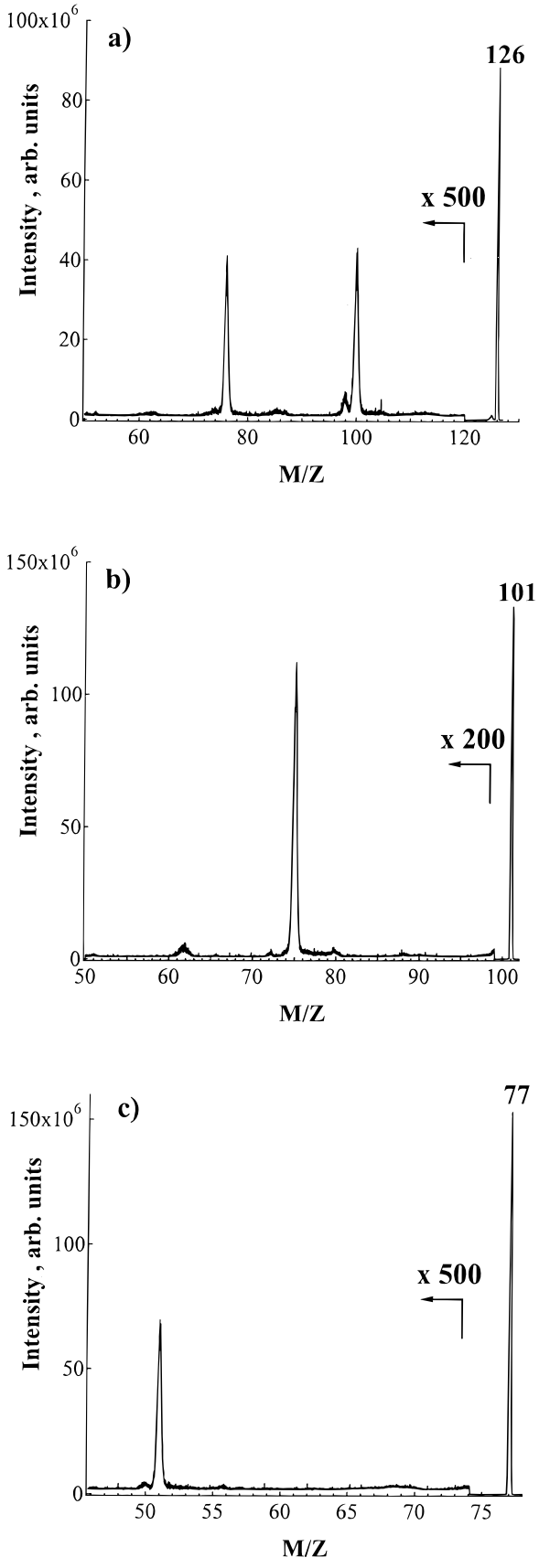

Figure 2. MIKEs spectra of (a) *m*/*z* 126, (b) *m*/*z* 101, and (c) *m*/*z* 77.

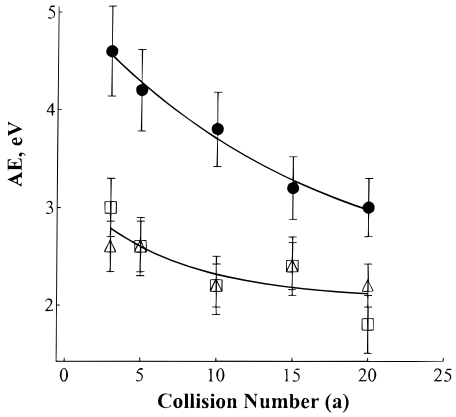

Figure 3. Relative appearance energies as a function of Ar pressure in the cell for *m*/*z* 101 (●), *m*/*z* 126 (□), and *m*/*z* 77 (△).

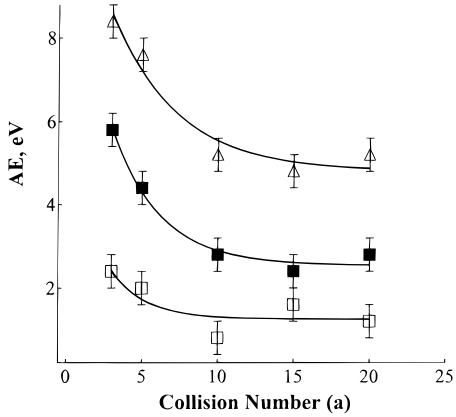

Figure 4. Relative appearance energies as a function of Ar pressure in the cell for *m*/*z* 51 (■), *m*/*z* 75 (□), and *m*/*z* 76 (△).

close to the intersection of $k(E)$ curves. Outside this window, only one of the products is observed. We infer that this explanation is the correct one for the absence of *m*/*z* 100 in SORI−CID spectra collected over a wide range of collision energies.

Appearance Energies. It has been shown previously that multiple collisions between an ion and neutral target cause experimental appearance energies (AEs) to shift toward lower values.[24−26] Thus absolute values of appearance energies obtained under multiple-collision conditions can be used only for qualitative analysis of experimental results. Vanishing current relative AEs of major CID fragments of bromonaphthalene are presented in Figures 3 and 4. The AEs of the corresponding precursor ions were subtracted from the absolute experimental values. For example, the relative appearance energy of $C_4H_3^+$ (*m*/*z* 51) was calculated as AE($C_4H_3^+$) − AE($C_6H_5^+$) − AE($C_{10}H_7^+$). The results indicate that reactions 2 and 4 (Scheme 1) have similar energetics, whereas the formation of $C_8H_5^+$ from naphthyl cation requires significantly higher excess internal energy. However, $C_8H_5^+$ (*m*/*z* 101) formed by reaction 3 (Scheme 1) is much less stable than other fragments from the same precursor ($C_{10}H_7^+$). As a result, the AE of $C_6H_3^+$ (*m*/*z* 75) formed from $C_8H_5^+$ is much lower than the AE of $C_4H_3^+$ (*m*/*z* 51) formed by reaction 4a (Scheme 1). Formation of $C_6H_4^+$, the lowest-energy fragment of $C_{10}H_6^+$, requires much higher energies than reactions 3a and 4a (Scheme 1).

Modeling of Fragmentation Efficiency Curves. Energy-resolved fragmentation efficiency curves were modeled using RRKM/QET calculations in the following way:

(1) The microcanonical rate coefficients $k(E)$ were calculated as a function of internal energy using the following microcanonical RRKM/QET expression:

$$k(E) = \frac{\sigma W^{\ddagger}(E - E_0)}{h\rho(E)} \tag{5}$$

where $\rho(E)$ is the density of states of the reactant, $W^{\ddagger}(E - E_0)$ is the sum of states of the transition state, E_0 is the critical energy, h is Plank's constant, and σ is the reaction path degeneracy.

(2) Fragmentation probability as a function of the internal energy of the parent ion and the experimental observation time (t_r), $F(E, t_r)$, was calculated from the rate−energy $k(E)$ dependencies. The function $F(E, t_r)$ is commonly referred to as a breakdown curve. A collection of breakdown curves, called the breakdown graph (BDG), was then constructed from the individual breakdown curves calculated for each reaction channel.

(3) The energy deposition function was described by the following analytical expression:

$$P(E,E_{CM}) = (E - \Delta)^l \exp(-(E - \Delta)/f(E_{CM}))/C \tag{6}$$

where l is a parameter, $C = \Gamma(l + 1)[f(E_{CM})]^{l+1}$ is a normalization factor, and $f(E_{CM})$ has the following form:

$$f(E_{CM}) = A_2 E_{CM}^{\ 2} + A_1 E_{CM} + E_{th}/(l + 1) \tag{7}$$

where A_1 and A_2 are parameters, and E_{th} is the average thermal energy at 298 K. This function, $P(E,E_{CM})$, is slightly different from the function used in our previous work.[26] An additional parameter Δ was introduced into the previously suggested functional form to improve the quality of the fits. [Although the expression used by us previously ($\Delta = 0$) provided an excellent fit to our experimental study of SORI excitation of $C_6H_5Br^{+\bullet}$, the additional parameter Δ was definitely required to fit the rather more complex dissociation of $C_{10}H_7Br^{+\bullet}$]. We have shown previously[26] that the proposed analytical form for the collisional energy deposition function has enough flexibility to reproduce experimental results obtained over a wide range of experimental parameters (e.g., collision energies and pressures). An exponential CEDF obtained with $l = 0$ can be used to model single-collision experiments, whereas Boltzmann-like CEDF (high values of l) can be utilized to reproduce multiple-collision experiments.

(4) Collisional activation produces ions with a wide distribution of internal energies, $P(E,E_{CM})$. The contribution of ions with internal energy E to the observed signal intensity for a particular reaction channel i equals $F_i(E, t_r)P(E, E_{CM})$. Integrating over internal energies yields an overall signal intensity at a given CM energy, $I(E_{CM})$:

$$I(E_{CM}) = \int_0^{\infty} F(E, t_r)P(E, E_{CM})\mathrm{d}E \tag{8}$$

Integration is performed from 0 to infinity because, in general, the ion can acquire rather high internal energy in multiple-collisions with neutral molecules.

The results were compared with the experimental FECs. The fitting parameters employed in the present modeling scheme include critical energies and entropies of different reaction channels, parameters used in eqs 6 and 7 for the energy deposition function, and the rate of radiative decay of the excited parent ion. These parameters were varied until the best fit to experimental fragmentation efficiency curves was obtained.

RRKM/QET Calculations. Reactions 1−4, 3a, and 4a from Scheme 1 were considered in the present modeling. The energetics and dynamics of reaction 1 were studied previously using time-resolved photodissociation (TRPD) and time-resolved photoionization mass spectrometry (TPIMS).[29] The critical energy (E_0) and activation entropy ($\Delta S^{\ddagger}$) that gave a best fit to the TRPD and TPIMS results were $E_0 = 3.23 \pm 0.07$ eV and $\Delta S^{\ddagger} = 7.7 \pm 2.5$ e.u.[29] RRKM parameters for reaction 4a were adopted from our study on the energetics of fragmentation of bromobenzene radical cation.[26] To the best of our knowledge, energetics of reactions 2−4 and 3a have not been studied previously.

RRKM calculations of the dissociation rate−energy curve of the molecular ion were carried out using neutral 1-bromonaphthalene frequencies.[30] The transition state frequencies were chosen as suggested by Gotkis et al.;[29] namely, the C−Br stretching mode (584 cm^{-1}) was chosen to represent the reaction coordinate and the frequencies of several other modes were varied to obtain the activation entropy of 7.7 e.u. Three vibrational frequencies associated with bromine atom were deleted to obtain vibrational frequencies of naphthyl cation ($C_{10}H_7^+$). In a similar way, vibrational frequencies of $C_8H_5^+$ were obtained from the frequencies of phenylacetylene radical cation.[31] Critical energies and transition state vibrational frequencies of reactions 2−4, 3a, and 4a were varied to get the best fit to the experimental fragmentation efficiency curves. The somewhat arbitrary choice of the transition state is acceptable because RRKM calculations are not sensitive to the details of vibrational frequencies of the molecular ion and the transition state but rather to the degree of tightness or looseness of the transition state, which is characterized by its activation entropy ($\Delta S^{\ddagger}$).[32]

Energy Partitioning. The internal energy of the fragments formed by reactions 1 and 2 can be estimated easily from the internal energy of a corresponding precursor ion under the logical premise that $Br^{\bullet}$ and $H^{\bullet}$ do not carry off any internal energy. However, the partitioning of energy between the ionic and neutral products must be considered to estimate the internal energy content of $C_8H_5^+$ formed by reaction 3 and $C_6H_4^+$ formed by reaction 4. If statistical partitioning of internal energy is assumed, the probability that for total internal energy E in the precursor ion an energy between ϵ and $\epsilon + d\epsilon$ remains internal energy of ionic fragment is given by:[33,34]

$$p(E, \epsilon) = \frac{\rho_1(\epsilon)\rho_2(E - E_0 - \epsilon)d\epsilon}{\int_0^{E-E_0} \rho_1(\epsilon)\rho_2(E - E_0 - \epsilon)d\epsilon} \qquad (9)$$

where ρ_1 and ρ_2 are the densities of states of ionic and neutral fragments, respectively, and E_0 is the critical energy for reaction. It should be mentioned that the general results of energy partitioning are not sensitive to the details of the vibrational frequencies.[36]

Vibrational frequencies of C_2H_2 and C_4H_2 (1,3-butadiyne) were adopted from ref 35. The probability distributions given by eq 9 were calculated for different internal energies of the precursor ion (E). The most probable internal energy deposited in the fragment ion of interest (E_{mp}) was extracted from each distribution. Figures 5a and 5b show the dependence of the most probable internal energy as a function of $E - E_0$. Two lines corresponding to ($E - E_0$) (dashed line) and ($E - E_0$)N_D/N_P (dotted line) are shown for comparison (N_D and N_P represent the number of internal degrees of freedom of the fragment ion and its precursor, respectively). The latter expression, ($E - E_0$)N_D/N_P, is commonly used for very simple estimation

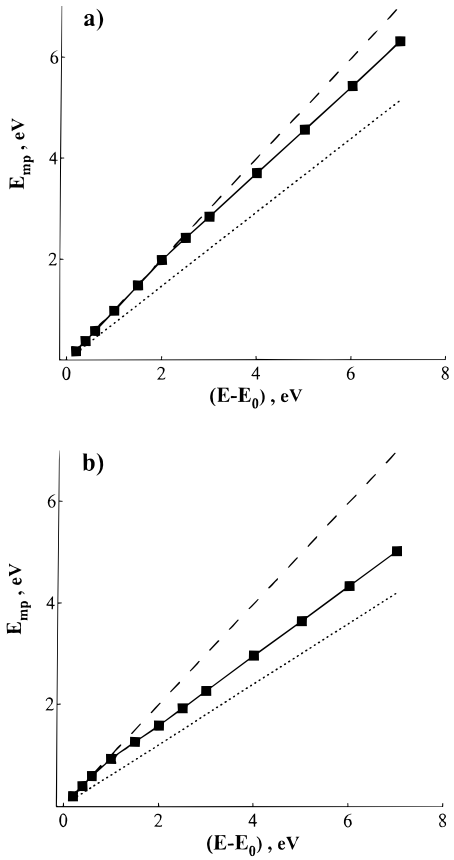

Figure 5. The most probable internal energy deposited into (a) $C_8H_5^+$ (reaction 3) and (b) $C_6H_5^+$ (reaction 4) as a function of $E - E_0$. Two lines corresponding to ($E - E_0$) (dashed line) and ($E - E_0$)N_D/N_P (dotted line) are shown for comparison. Here, N_D and N_P represent the number of internal degrees of freedom of the fragment ion and its precursor, respectively.

of the energy partitioning among fragments. Our calculations indicate that for low internal energies, E_{mp} closely follows the line corresponding to ($E - E_0$), whereas for higher energies, E_{mp} deviates from the ($E - E_0$) line. The extent of the deviation is governed by the number of degrees of freedom of the ionic and neutral fragments formed in reaction. Thus, the deviation is relatively small for reaction 3, where a large ion ($C_8H_5^+$) and a small neutral molecule (C_2H_2) are formed, whereas a substantial deviation from the ($E - E_0$) line is obtained for reaction 4. In this case, the ionic fragment ($C_6H_5^+$) is much smaller and the neutral fragment (C_4H_2) is larger than the corresponding fragments formed by reaction 3. For each reaction, the dependencies of E_{mp} on $E - E_0$ were fitted with a second-order polynomial, and the analytical functional form obtained in this way was used to calculate the internal energy of $C_8H_5^+$ and $C_6H_5^+$ throughout the RRKM calculations.

Results of Theoretical Modeling

Dissociation Energetics. Fragmentation efficiency curves for reactions 1−4, 4a, and 3a were modeled in the present study. Intensities of subsequent fragments of m/z 126 were added to the FECs of $C_{10}H_6^{+\bullet}$. As previously described, double-resonance experiments revealed that m/z 74 is formed mainly from m/z 75, whereas m/z 50 is formed from m/z 51. Thus, FECs of m/z 75 and 74, and m/z 51 and 50 were added together.

RRKM parameters—the critical energies and activation entropies that give the best fit to the whole set of experimental fragmentation efficiency curves (FECs)—are summarized in

TABLE 1: RRKM/QET Parameters

Reaction	E_0, eV	$\Delta S^{\ddagger}$, e.u.
1	3.2	7.7
2	4.1 ± 0.2	-0.1 ± 0.7
3	4.6 ± 0.2	7.8 ± 2
4	4.3 ± 0.2	6.4 ± 2
3a	3.3 ± 0.3	8.1 ± 0.7
4a	3.9 ± 0.2	7.6 ± 0.7

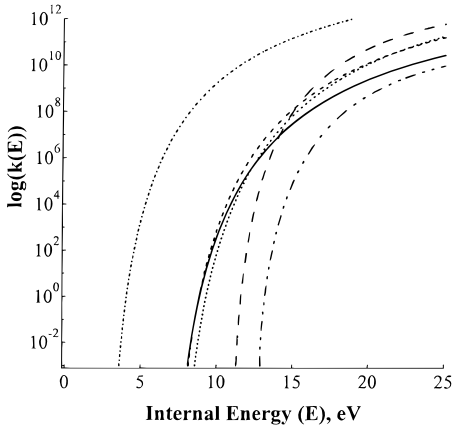

Figure 6. RRKM rate−energy curves corresponding to the present model: (-·-·-) reaction 1; (—) reaction 2; (·····) reaction 3; (- - -) reaction 4; (- - -) reaction 3a; (-·-·-·) reaction 4a.

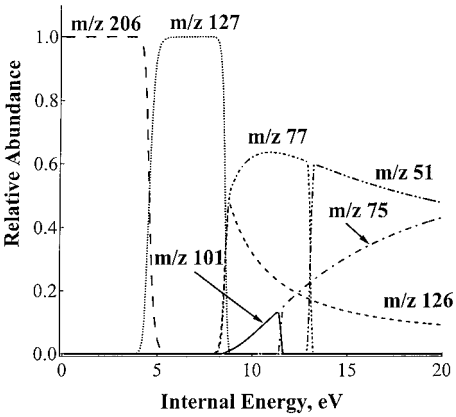

Figure 7. Calculated breakdown curves for reactions 1−4, 3a, and 4a (the experimental reaction time is 5 s).

Table 1. Rate−energy dependencies for all reactions included in the modeling are shown in Figure 6. The radiative decay rate that gave the best agreement with the experimental FECs is 90 ± 5 s^{-1}. Calculated FECs were not very sensitive to activation entropies, except for competing reactions 2−4, where both critical energies and activation entropies were very important.

Breakdown curves presented in Figure 7 were calculated from the rate−energy dependencies at 0 K for a reaction time of 5 s, the time sampled in our experiments. Because these reactions have very similar energetic requirements, breakdown curves of *m*/*z* 126 and 77 are very close to each other at low internal energies. As the internal energy increases, the microcanonical rate constants for reactions 2 and 4 diverge, significantly reflecting the differences in their activation entropies. As a result, the relative abundance of $C_{10}H_6^+$ (*m*/*z* 126) drops dramatically. It follows that relative intensities of all the fragments having this ion as a precursor will be low. Because reaction 3 has a higher critical energy than reactions 2 and 4, the amount of *m*/*z* 101 produced at low internal energies is very small. However, reaction 3 has a high activation entropy and the

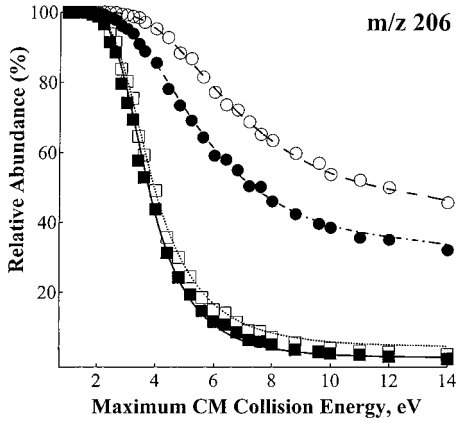

Figure 8. SORI−CID fragmentation efficiency curves *m*/*z* 206 and results of theoretical modeling: (○, - - -) $a = 3$; (●, -·-·-) $a = 5$; (□, ·····) $a = 15$; (■, —) $a = 20$.

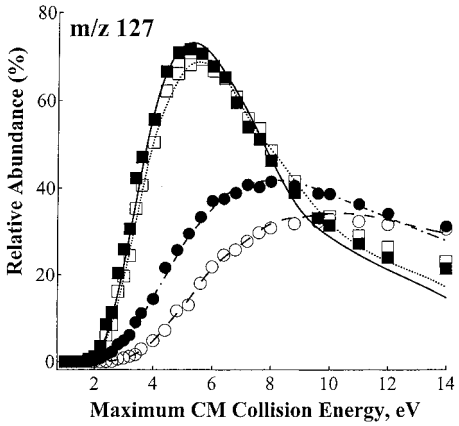

Figure 9. SORI−CID fragmentation efficiency curves *m*/*z* 127 and results of theoretical modeling: (○, - - -) $a = 3$; (●, -·-·-) $a = 5$; (□, ·····) $a = 15$; (■, —) $a = 20$.

relative abundance of *m*/*z* 101 rises with internal energy. Subsequent fragmentation of $C_8H_5^+$ requires much less energy than fragmentation of $C_6H_5^+$. It follows that relatively small amount of $C_8H_5^+$ (*m*/*z* 101) is formed at any collision energy. At high collision energies, $C_8H_5^+$ is efficiently converted to $C_6H_3^+$ and we predict an intense peak at *m*/*z* 75. All these predictions are in perfect agreement with experimental results. Experimental and calculated fragmentation efficiency curves are compared in Figures 8−14. The agreement between the model and the experiment is quite satisfactory for all reactions included in the modeling.

Because the critical parameters for reaction 1 are well established,[29] we used the fixed values of critical energy ($E_0 = 3.23$ eV) and activation entropy ($\Delta S^{\ddagger} = 7.7$ e.u.) for this reaction throughout the fitting procedure. To test the uniqueness of the fits, the critical energy of reaction 2 was systematically changed in increments of 0.05 eV and the rest of the fitting parameters were adjusted to give the best fit. This test revealed that the fits are unique within the error limits given in Table 1.

Although the fragmentation of naphthalene has been studied quite extensively, little is known about the fragmentation of naphthyl cation ($C_{10}H_7^+$). The major dissociation products of $C_{10}H_7^+$ observed in the present study correspond to the loss of H, C_2H_2, and C_4H_2. The loss of molecular hydrogen giving rise to a peak at *m*/*z* 125 was also observed. However, the intensity of *m*/*z* 125, when present, was just above the noise level.

Dissociation thresholds for reactions 1−4, 3a, and 4a are summarized in Table 1. The dissociation threshold for reaction

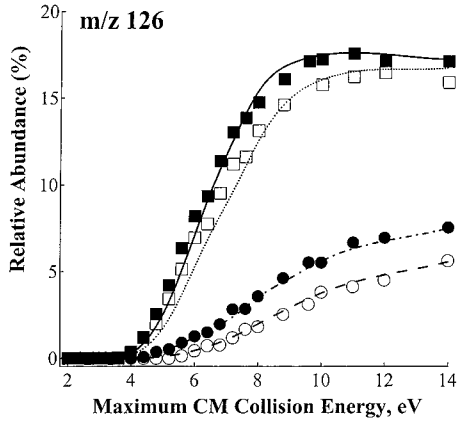

Figure 10. SORI−CID fragmentation efficiency curves *m*/*z* 126 and results of theoretical modeling: (O, - - -) $a = 3$; (●, -·-·-) $a = 5$; (□, ·····) $a = 15$; (■, —) $a = 20$.

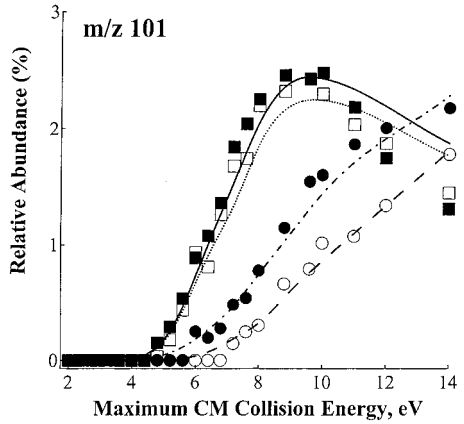

Figure 11. SORI−CID fragmentation efficiency curves *m*/*z* 101 and results of theoretical modeling: (○, - - -) $a = 3$; (●, -·-·-) $a = 5$; (□, ·····) $a = 15$; (■, —) $a = 20$.

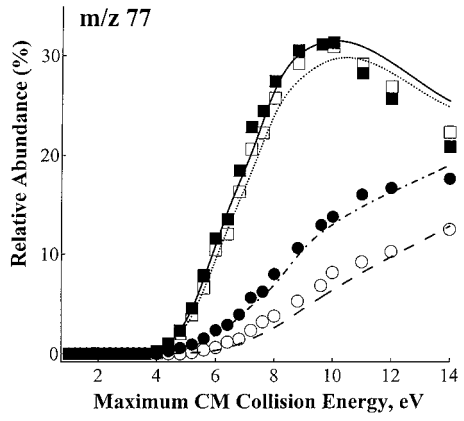

Figure 12. SORI−CID fragmentation efficiency curves *m*/*z* 77 and results of theoretical modeling: (○, - - -) $a = 3$; (●, -·-·-) $a = 5$; (□, ·····) $a = 15$; (■, —) $a = 20$.

4 can be estimated using a simple thermochemical cycle based on the following reactions:

$$C_{10}H_8^{+\bullet} \rightarrow C_{10}H_7^{+} + H^{\bullet} \quad (10)$$

$$C_{10}H_7^{+} \rightarrow C_6H_5^{+} + C_4H_2 \quad (4)$$

$$C_6H_6^{+\bullet} \rightarrow C_6H_5^{+} + H^{\bullet} \quad (11)$$

In this case, the critical energy of reaction 4, $E_0(4)$, can be expressed in terms of critical energies for reactions 10 and 11

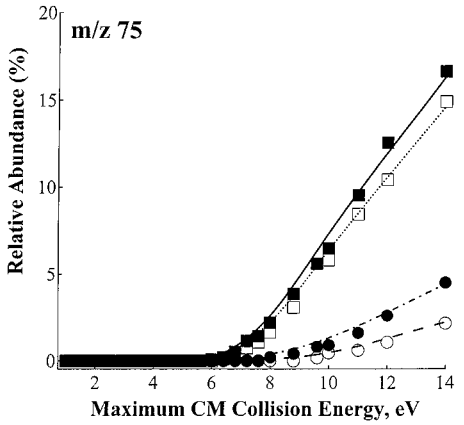

Figure 13. SORI−CID fragmentation efficiency curves *m*/*z* 75 and results of theoretical modeling; (○, - - -) $a = 3$; (●, -·-·-) $a = 5$; (□, ·····) $a = 15$; (■, —) $a = 20$.

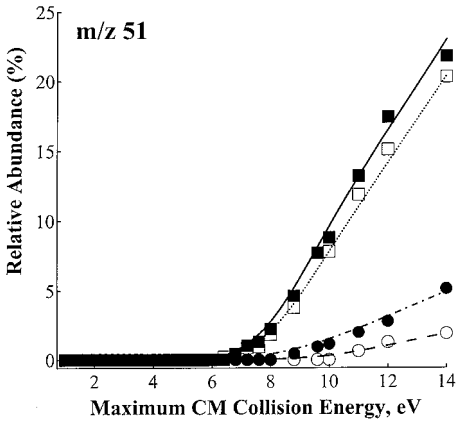

Figure 14. SORI−CID fragmentation efficiency curves *m*/*z* 51 and results of theoretical modeling: (O, - - -) $a = 3$; (●, -·-·-) $a = 5$; (□, ·····) $a = 15$; (■, —) $a = 20$.

TABLE 2: Thermochemical Data

Formula	ΔH_f^0(0 K), kcal/mol	Reference
$C_{10}H_8^{+\bullet}$ (naphthalene)	229.2	31
$C_6H_6^{+\bullet}$ (benzene)	237.2	31
C_4H_2 (1,3-Butadiyne)	110.8	37
C_2H_2	54.2	37
$H^{\bullet}$	52.1	37
$C_{10}H_7^{+}$	281 ± 3	29
$C_{10}H_6^{+\bullet}$	323 ± 5	This work
$C_8H_5^{+}$	333 ± 5	This work

[$E_0(10) = 4.48$ eV and $E_0(11) = 3.7$ eV[40]] and the heats of formation of $C_{10}H_8^{+\bullet}$, $C_6H_6^{+\bullet}$, and C_4H_2 in the following way:

$$E_0(4) = E_0(11) - E_0(10) + \Delta H_f^0(C_6H_6^{+\bullet}) + \Delta H_f^0(C_4H_2) - \Delta H_f^0(C_{10}H_8^{+\bullet}) = 4.36 \text{ eV}$$

The critical energy derived from our modeling $E_0(4) = 4.3 \pm 0.2$ eV is in excellent agreement with this estimated value. The critical energy for reaction 4a is 3.9 ± 0.2 eV. This value is the same within the error limits as the dissociation threshold for this reaction obtained in our previous study on the fragmentation of bromobenzene.[26]

Table 2 summarizes thermochemical data used for estimating threshold energies as well as heats of formation of $C_{10}H_6^{+\bullet}$ and $C_8H_5^{+}$ obtained in the present study. Heats of formation can be determined from dissociation thresholds fairly accurately, provided the reaction proceeds via a loose transition state. The

activation entropy for reaction 3 found from the modeling is 7.8 ± 2 e.u., corresponding to a loose transition state. However, reaction 2 has lower activation entropy (-0.1 ± 0.7 e.u.). Consequently, the heat of formation determined for $C_{10}H_6^{+\bullet}$ could be slightly overestimated; the activation energy for the back reaction is unknown.

The lowest-energy dissociation channel of naphthyl cation is the loss of a hydrogen atom, which has a critical energy of 4.1 eV. The dissociation threshold for acetylene loss is 0.5 eV higher (4.6 eV), whereas the loss of C_4H_2 requires 4.3 eV. The relative energies for naphthyl fragmentation are apparently different from the relative energies reported for $C_{10}H_8^{+\bullet}$. First of all, the loss of acetylene and hydrogen from $C_{10}H_7^+$ has very different energetic requirements. In contrast, these two reactions have similar threshold energies when the precursor is $C_{10}H_8^{+\bullet}$. Furthermore, loss of C_4H_2 from $C_{10}H_7^+$ is much faster than the corresponding loss from naphthalene radical cation.

It would be interesting to compare the fragmentation energetics of naphthyl cation and naphthalene radical cation. Several groups have studied fragmentation of naphthalene radical cation both experimentally and theoretically.[38−43] Jochims et al. have studied the photofragmentation of naphthalene and azulene monocations over the excitation energy range 7−22 eV.[38] The major low-energy products of $C_{10}H_8^{+\bullet}$ correspond to the loss of H, H_2, C_2H_2, and C_4H_2. They showed that identical products are formed from these species, suggesting azulene and naphthalene fragmentation occurs through formation of a common intermediate. Experimental appearance energies for hydrogen and acetylene loss from naphthalene are identical, whereas loss of H_2 and C_4H_2 requires 0.3 eV higher energy. Ho et al. reported time-resolved photodissociation studies of naphthalene and naphthalene-d_8 ions.[40] Bond energies of 4.48 eV for H loss and 4.41 eV for acetylene loss were derived from RRKM modeling of their experimental data.

Evidently, the mechanism of fragmentation of naphthyl cation is quite different from the mechanism of fragmentation of naphthalene cation.

Dissociation Mechanisms. Simple bond cleavage leads to a loss of a hydrogen atom from the naphthyl cation. The critical energy for hydrogen loss from $C_{10}H_7^+$ (4.1 eV) is lower than the critical energy for hydrogen loss from $C_{10}H_8^{+\bullet}$ (4.48 eV),[40] reflecting the relative stabilities of the respective parent ions. Schemes 2 and 3 show the proposed fragmentation mechanisms for reactions 3 and 4 that can rationalize differences in dissociation mechanisms of $C_{10}H_7^+$ and $C_{10}H_8^{+\bullet}$. Charge-site-initiated cleavage of two C−C bonds can lead to the loss of C_2H_2 from the naphthyl cation (Scheme 2). Heterolytic cleavages are known to be energetically less favorable than radical-site reactions,[44] which explains the higher critical energy for acetylene loss obtained in the present study.

Because heats of formation of different possible isomers of $C_8H_5^+$ have not been determined previously, we cannot distinguish between them based on the heat of formation obtained from the modeling (Table 2). However, some information on the possible structure of $C_8H_5^+$ could be obtained from comparison with $C_8H_6^{+\bullet}$. Theoretical calculations on the relative stability of different isomers of $C_8H_6^{+\bullet}$ have shown[31,41] that benzocyclobutadiene radical cation (**1**) is ~4 kcal/mol more stable than phenylacetylene radical cation (**2**) and proposed that **1** is the most plausible product of naphthalene fragmentation. The structure of $C_8H_6^{+\bullet}$ formed from different precursors was probed using different mass spectrometric techniques, such as collisional activation, neutralization reionization, and charge reversal.[42] It has been proved experimentally that loss of acetylene does not lead to **2** as a major product. The experimental results were shown to be in accord with the formation of **1**. However, formation of an open-chain isomer [octa-3,5-diene-1,7 diyne **3**] could not be ruled out.

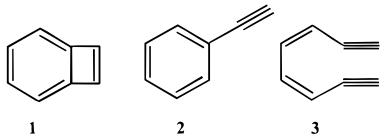

1 **2** **3**

Charge-induced fragmentation of naphthyl cation, outlined in Scheme 2, can lead to both phenylacetylene-like (**2**) and benzocyclobutadiene-like (**1**) structures of $C_8H_5^+$.

SCHEME 2

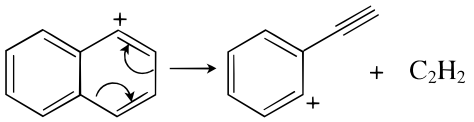

The structure of $C_6H_5^+$ formed by reaction 4 in not known. However, the subsequent dissociation of this ion follows the same pathway as the dissociation of phenyl cation formed from $C_6H_5Br^{+\bullet}$;[24] namely, $C_6H_5^+$ undergoes acetylene loss followed by hydrogen elimination. Thus, we believe that the loss of C_4H_2 from naphthyl cation leads to formation of the phenyl cation. Formation of phenyl cation and stable 1,3-butadyine molecule from $C_{10}H_7^+$ implies a more complex mechanism with 1,2- and 1,4-hydrogen migrations (Scheme 3). We suggest that the

SCHEME 3

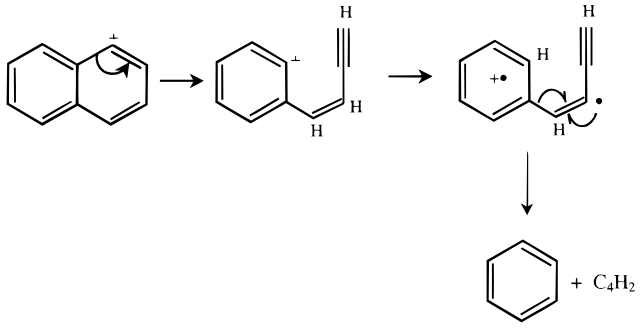

opening of the ring occurs through a charge-site-initiated cleavage of the indicated C−C bond. One hydrogen atom is donated from the open chain to the ring followed by radical-site-initiated cleavage of a second C−C bond. Because only one charge-site-initiated cleavage is involved in this process and because hydrogen shift to the ring requires less energy than the dissociation threshold,[43] this reaction is faster than the loss of acetylene from $C_{10}H_7^+$.

Energy Transfer Efficiency. The average energy transferred upon collisions is shown in Figure 15 as a function of maximum center-of-mass energy for different pressures. The average energy rises nearly linearly at low collision energies and less that linearly at higher energies. When the collision number increases from 3 (lowest curve) to 5, energy transfer exhibits the anticipated strong increase. It increases again as the collision number increases to 15 but has "saturated" such that no further increase is discernible as the collision number increases from 15 to 20. Similar behavior of the average internal energy versus collision energy was observed by Lee et al. for collisional excitation of $CH_4^{+\bullet}$,[45] by Wysocki et al. for $(C_2H_5)_4Si^{+\bullet}$,[46] and by Laskin et al. for $C_6H_5Br^{+\bullet}$.[26] The essential coalescence of

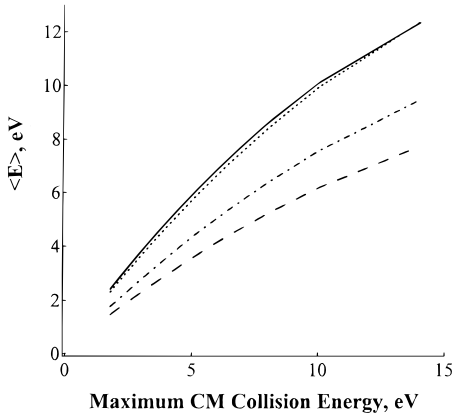

Figure 15. Average internal energy transferred upon collisions as a function of the maximum center-of-mass energy of parent ion at different pressures: (- - -) $a = 3$; (-•••-) $a = 5$; (•••••••) $a = 15$; (—) $a = 20$.

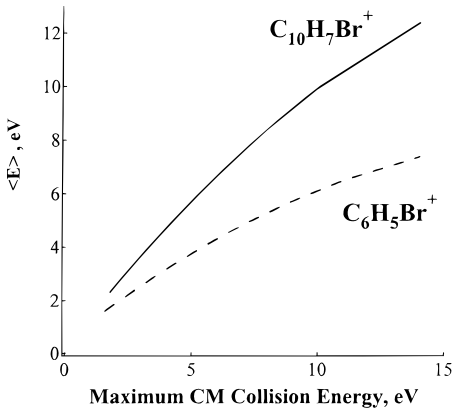

Figure 16. Average internal energy transferred following collisions as a function of the maximum center-of-mass energy of parent ion for (- - -) bromobenzene and (—) bromonaphthalene obtained at the same pressure, giving rise to a collision number $a = 15$.

the two curves corresponding to $a = 15$ and $a = 20$ was noted in our previous study of SORI−CID of bromobenzene, where we demonstrated the same saturation effect with increasing collision number.

Comparison between the average energy deposited upon SORI excitation of $C_6H_5Br^{+\bullet}$ and $C_{10}H_7Br^{+\bullet}$ for $a = 15$ is shown in Figure 16. Significantly higher average internal energies are deposited into the larger ion. Assuming that internal energy distribution of parent ion is close to a thermal distribution, the average internal energy can be expressed as an "effective temperature". Figures 17a and 17b show a comparison between effective temperatures of bromobenzene and bromonaphthalene at two pressures corresponding to 5 and 15 collisions. Although the average energies deposited into these ions are very different, the "effective temperatures" are the same. As mentioned earlier, an analogous result was obtained from the comparison of BIRD and SORI−CID fragmentation kinetics of protonated leucine enkephalin and doubly protonated bradykinin.[24] However, this comparison suffered from a limited temperature range (~476 K). In contrast, the "effective temperatures" of bromonaphthalene ions ranged from 1000 to 3700 K as the maximum SORI center-of-mass collision energy was increased to 15 eV. The temperature range sampled in the present study significantly exceeds that accessible by BIRD, and no calibration of the "effective temperature" obtained following SORI excitation with true blackbody temperature is possible.

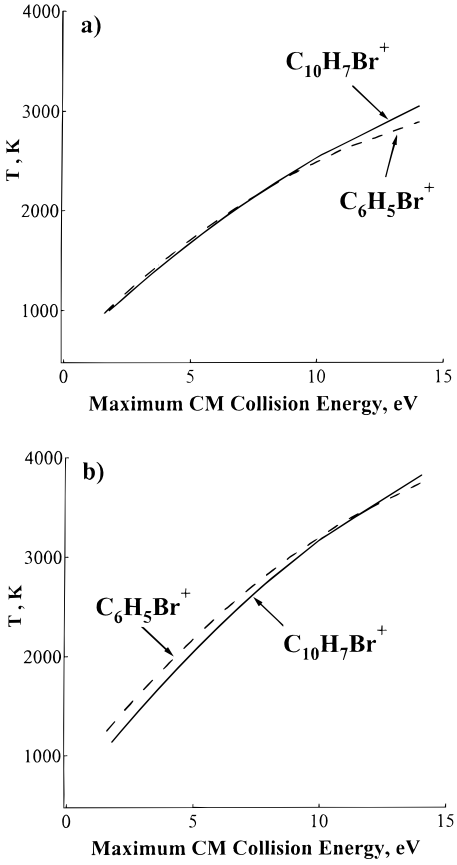

Figure 17. Effective temperature as a function of the maximum center-of-mass energy of parent ion for (- - -) bromobenzene and (—) bromonaphthalene at two different pressures: (a) $a = 5$, and (b) $a = 15$.

Conclusions

This work presents a detailed study of the fragmentation of 1-bromonaphthalene radical cation following SORI excitation. Bromonaphthalene radical was chosen as a logical extension of our previous study of the fragmentation of bromobenzene radical cation. The similarity of these two systems arises from the same initiation step for fragmentation; that is, bromine loss from the molecular ion. The differences reflect the more complex nature of dissociation of naphthyl cation as compared with phenyl cation. The fragmentation energetics of phenyl cation, previously studied by us, was logically incorporated into the modeling scheme employed in the present investigation. Because the energetics and dynamics of naphthalene radical cation dissociation are better characterized using various experimental and theoretical approaches than the fragmentation of $C_{10}H_7Br^{+\bullet}$, it would be desirable to investigate naphthalene cation fragmentation using the same methods. Unfortunately, this is not possible because the resonance frequencies of $C_{10}H_8^{+\bullet}$ and $C_{10}H_7^+$ are too close together to excite only $C_{10}H_8^{+\bullet}$ using SORI excitation.

Fragmentation efficiency curves (FECs) of the parent ion and six major fragments obtained at different pressures were successfully modeled using the general approach proposed previously.[26] Good agreement between experiment and model was found for all the fragment ions. An additional parameter was introduced into the analytical expression for the collision energy deposition function (eq 6) to achieve a better fit to the experimental data. Critical energies and activation entropies for reactions 1−4, 3a, and 4a were obtained from the RRKM

modeling. Calculated FECs were not sensitive to the activation entropies of reactions 1, 3a, and 4a. However, modeling results were highly sensitive to the activation entropies of competing reactions 2−4. We have shown that the partitioning of energy between the ionic and neutral products must be included in this work to model the fragmentation kinetics of a complex system. This was done assuming that the excess energy is partitioned statistically among the fragments and calculating all the permutations of the energy partitioning from densities of states of the ionic and neutral fragments.

The critical energies obtained from the best fit were compared with the literature values or thermochemical estimates whenever possible. Dissociation thresholds obtained using the present approach are in excellent agreement with literature values. We infer that the present approach can be utilized to study the energetics and dynamics of complex systems. Uncertainty in critical energies obtained in the present study is comparable to the uncertainties commonly obtained using photoionization or photodissociation techniques, which are the best well-characterized methods for studying the energetics of ionic fragmentation. This very encouraging result leads us to extend this approach to the fragmentation of large molecules (e.g., peptides) for which the use of photoionization techniques is very limited.

It is clear that there are several parameters that are optimized based on experimental data, and the question arises whether alternate formalism or a different combination of parameters would provide an equivalent or superior rationalization of energy deposition in SORI excitation. Because the kinetics description is physically correct, we have examined the sensitivity of the fit to choice of energetics parameters. The sensitivity test described earlier confirmed the uniqueness of the fitting parameters presented in Table 1.

We have shown that the average energy deposited into the bromonaphthalene radical cation following SORI excitation is significantly higher than the average energy deposited into bromobenzene radical cation. However, the effective temperatures, derived from the average internal energies, are the same for $C_6H_5Br^{+\bullet}$ and $C_{10}H_7Br^{+\bullet}$. The effective temperature of excited ions is determined by the SORI conditions, namely the center-of-mass collision energy and pressure. The effective temperature of precursor ion varied between 1000 and 3700 K under the experimental conditions employed in this study. An advantage of collisional activation under multiple-collision conditions is that a very wide range of effective temperatures can be easily covered within the same experimental setup. Moreover, the suggested modeling approach does not require a priori knowledge of the effective temperature, which eliminates the necessity of any additional calibration of effective temperature of SORI-excited ions utilizing BIRD or the master equation approach for modeling internal energy distributions.

Acknowledgment. This research was supported in part by NSF grants CHE-9616711 and CHE-9634238 and by DOE grant DE-FG02-97ER14813. We thank Professor D. P. Ridge, Professor C. Lifshitz, Dr. A. Laskin, Dr. A. Shukla, and Dr. M. Byrd for very helpful discussions.

References and Notes

(1) McLuckey, S. A. *J. Am. Soc. Mass Spectrom.* **1992**, *3*, 599.
(2) Shukla, A. K.; Futrell, J. H. *Mass Spectrom. Rev.* **1993**, *12*, 211.
(3) Hayes, R. N.; Gross, M. L. In: *Methods in Enzymology*, Vol. 193: Mass Spectrometry, McCloskey, J. A.; Ed., Academic Press: Orlando, 1990, Chapter 10.
(4) Marzluff, E. M.; Beauchamp, J. L. In: *Large Ions: Their Vaporization, Detection and Structural Analysis*; Baer, T.; Ng, C. Y.; Powis, I., Eds.; Wiley: New York, 1996; Chapter 5.
(5) Cody, R. B.; Burnier, R. C.; Freiser, B. S. *Anal. Chem.* **1982**, *54*, 96.
(6) Carlin, T. J.; Freiser, B. S. *Anal. Chem.* **1983**, *55*, 571.
(7) Lee, S. A.; Jiao, C. Q.; Huang, Y.; Freiser, B. S. *Rapid Commun. Mass Spectrom.* **1993**, *7*, 819.
(8) Williams, E. R.; McLafferty, F. W. *J. Am. Soc. Mass Spectrom.* **1990**, *1*, 427.
(9) Gauthier, J. W.; Trautman, T. R.; Jacobson, D. B. *Anal. Chim. Acta* **1991**, *246*, 211.
(10) Boering, K. A.; Rolfe, J.; Brauman, J. I. *Rapid Commun. Mass Spectrom.* **1992**, *5*, 406.
(11) Boering, K. A.; Rolfe, J.; Brauman, J. I. *Int. J. Mass Spectrom. Ion Processes* **1992**, *117*, 357.
(12) Klassen, J. S.; Kebarle, P. *J. Am. Chem. Soc.* **1997**, *119*, 6552.
(13) Vékey, K.; Somogyi, Á.; Wysocki, V. H. *Rapid Commun. Mass Spectrom.* **1996**, *10*, 911.
(14) Lim, H.; Schultz, D. G.; Yu, C.; Hanley, L. *Anal. Chem.* **1999**, *71*, 2307.
(15) Freitas, M. A.; Hendrickson, C. L.; Marshall, A. G. *Rapid Commun. Mass Spectrom.* **1999**, *13*, 1639.
(16) Vachet, R. W.; Glish, G. L. *J. Am. Soc. Mass Spectrom.* **1998**, *9*, 175.
(17) Dunbar, R. C. *J. Phys. Chem.* **1994**, *98*, 8705.
(18) Price, W. D.; Schnier, P. D.; Williams, E. R. *Anal. Chem.* **1996**, *68*, 859.
(19) Price, W. D.; Schnier, P. D.; Jockusch, R. A.; Strittmatter, E. F.; Williams, E. R. *J. Am. Chem. Soc.* **1996**, *118*, 10640.
(20) Dunbar, R. C.; McMahon, T. B. *Science* **1998**, *279*, 194 and references therein.
(21) Dunbar, R. C.; McMahon, T. B.; Thölmann, D.; Tonner, D. S.; Salahub, D. R.; Wei. D. *J. Am. Chem. Soc.* **1995**, *117*, 12819.
(22) Price, W. D.; Schnier, P. D.; Williams, E. R. *J. Phys. Chem. B* **1997**, *101*, 664.
(23) Schnier, P. D.; Price, W. D.; Jockusch, R. A.; Williams, E. R. *J. Am. Chem. Soc.* **1996**, *118*, 7178.
(24) Schnier, P. D.; Jurchen, J. C.; Williams, E. R. *J. Phys. Chem. B* **1999**, *103*, 737.
(25) Fujiwara, M.; Naito, Y. *Rapid Commun. Mass Spectrom.* **1999**, *13*, 1633.
(26) Laskin, J.; Byrd, M.; Futrell, J. H. *Int. J. Mass Spectrom. Ion Processes* **2000**, *195/196*, 285.
(27) Hop, C. E. C. A.; McMahon, T. B.; Willett, G. D. *Int. J. Mass Spectrom. Ion Processes* **1990**, *101*, 191.
(28) Sievers, H. L.; Grützmacher, H.-F.; Caravatti, P. *Int. J. Mass Spectrom. Ion Processes* **1996**, *157/158*, 233.
(29) Gotkis, Y.; Naor, M.; Laskin, J.; Lifshitz, C.; Faulk, J. D.; Dunbar, R. C. *J. Am. Chem. Soc.* **1993**, *115*, 7402.
(30) Singh, S. N.; Bhatti, H. S.; Singh, R. D. *Spectrochim. Acta* **1978**, *34*, 985.
(31) Ling, Y.; Martin, J. M. L.; Lifshitz, C. *J. Phys. Chem.* **1997**, *101*, 219.
(32) Lifshitz, C. *Adv. Mass Spectrom.* **1989**, *11*, 113.
(33) Vestal, M. L. *J. Chem. Phys.* **1965**, *43*, 1356.
(34) Bente, III, P. F.; McLafferty, F. W.; McAdoo, D. J.; Lifshitz, C. *J. Phys. Chem.* **1975**, *79*, 713.
(35) Shimanouchi, T. Tables of Molecular Vibrational Frequencies Consolidated Volume I, National Bureau of Standards, 1972.
(36) Lin, Y. N.; Rabinovitch, B. S. *J. Phys. Chem.* **1970**, *74*, 1769.
(37) NIST Standard Reference Database 69 − November 1998 Release: NIST Chemistry WebBook.
(38) Jochims, H. W.; Rasekh, H.; Rühl, E.; Baumgärtel, H.; Leach, S. *Chem. Phys.* **1992**, *168*, 159.
(39) Gotkis, Y.; Oleinikova, M.; Naor, M.; Lifshitz, C. *J. Phys. Chem.* **1993**, *97*, 12282.
(40) Ho, Y.-P.; Dunbar, R. C.; Lifshitz, C. *J. Am. Chem. Soc.* **1995**, *117*, 6504.
(41) Granucci, G.; Ellinger, Y.; Boissel, P. *Chem. Phys.* **1995**, *191*, 165.
(42) Schroeter, K.; Schröder, D.; Schwarz, H. *J. Phys. Chem. A* **1999**, *103*, 4174.
(43) Koster, G.; Martin, J. M. L.; Lifshitz, C. *Perkin Trans. 2* **1999**, *11*, 2383.
(44) McLafferty, F. W.; Tureèek, F. *Interpretation of Mass Spectra*; University Science Books: Mill Valley, CA, 1993.
(45) Lee, S. H.; Kim, M. S.; Beynon, J. H. *Int. J. Mass Spectrom. Ion Processes* **1987**, *75*, 83.
(46) Wysocki, V. H.; Kenttämaa, H. I.; Cooks, R. G. *Int. J. Mass Spectrom. Ion Processes* **1987**, *75*, 181.
(47) Gorshkov, M. V.; Pasa-Tolic, L.; Smith, R. D. *J. Am. Soc. Mass Spectrom.* **1999**, *10*, 15.